To be published in Nucl. Inst. & Meth. Sect. B, April 2000

On the origin of surface smoothing by energetic cluster impact: molecular dynamics simulation and mesoscopic modeling

Michael Moseler,
School of Physics, Georgia Institute of Technology,
Atlanta, Georgia, 30332-0430

Oliver Rattunde, Johannes Nordiek, and Hellmut Haberland
Freiburg Materials Research Center, Stefan–Meier-Str. 21, D-79104 Freiburg, Germany

December 3, 1999

Abstract

Energetic cluster impacts have been applied for the production of high quality thin films as well as a tool for smoothing rough surfaces. Molecular dynamic simulations of cluster-surface collisions provide the following picture for the underlying microscopic mechanism: the impact of an energetic cluster onto a tilted part of the substrate induces a downhill particle current (consisting of both cluster and surface atoms) transfering the higher lying parts of the surface profile into the valleys. This effect is more pronounced for high kinetic energies. Based on these microscopic results, a mesoscopic model employing stochastic differential equations has been formulated allowing a quantitative explanation of experimental results from atomic force microscope measurements.

1 Introduction

Usually, thin films are produced by the deposition of atoms or molecules onto a solid substrate. The particles coming out of a gas or a molecular beam are randomly scattered over the surface thus leading to local fluctuations in the deposition rate. Without additional lateral transport processes, this irregular precipitation inevitably causes surface roughness. An activation energy is necessary for the lateral displacement of matter. Therefore, in physical vapour deposition technologies, the substrate is heated to several hundred degrees in order to stimulate enhanced surface diffusion. For materials which are not resistant to such high temperatures, the activation energy can also be supplied by particle bombardement [1]. A number of surface processing techniques uses a cluster beam instead of single atoms. Some examples, such as shallow implantation, erosion or micromachining are described in [2].

Energetic Cluster Impact (ECI) deposition [3] is especially suited to produce high quality films. In this technique, charged clusters are accelerated by an electric field of some keV and directed onto the substrate. In this way, huge amounts of mass and energy can be deposited locally, forming compact and almost atomically smooth thin films. From experimental observations it is obvious that the impact energy plays a key role in this technology and strongly influences the roughness of the films (fig. 1). For a further optimization of this method, it is necessary to understand the underlying microscopic

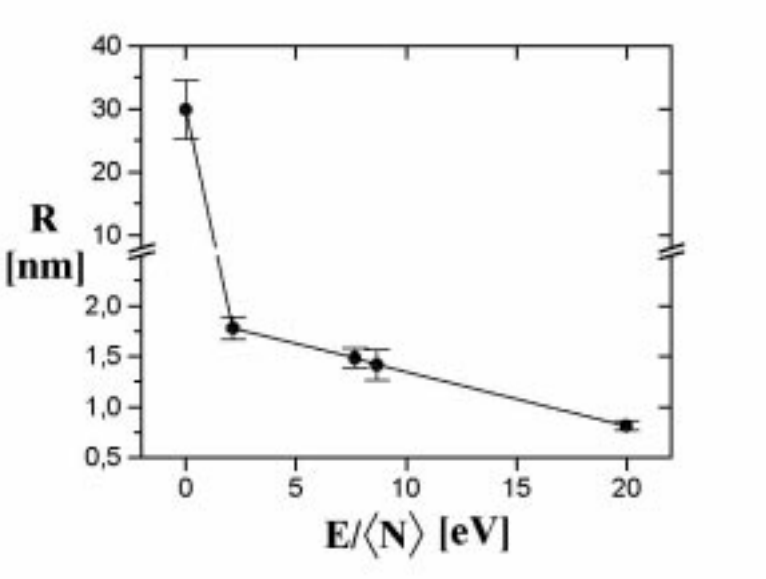

Figure 1: RMS roughness measured by atomic force microscopy as a function of impact energy per atom for thin films from Al_{2000} clusters. See section 3.7 for details.

mechanisms. This would help to elucidate the question how the mesoscopic properties like RMS roughness can be controlled.

Classical molecular dynamics (MD) proved an excellent tool for the investigation of cluster-surface collisions. The first calculations were made by Müller [4] with a two-dimensional model using Lennard-Jones potentials. In the following, three-dimensional simulations with small silicon [5] and metal clusters [6, 7] were performed. More exotic material combinations like Argon clusters impinging on NaCl surfaces were studied [8]. Meanwhile, a huge amount of literature has been produced dealing mainly with small cluster sizes [9]. Because a typical cluster used in ECI-deposition consists of thousands of atoms, we started to investigate the impact of large clusters with surfaces [10] and achieved a first qualitative understanding of the relationship between roughness and impact energy [11, 12].

Roughness of a film is a property of its height profile and may be observed on different lateral length scales [13]. MD provides information only on the nanometer-scale. On the other hand, for most technological applications roughness on a mesoscopic scale (several hundreds of nanometers) is of major importance. Also, experimental surface profiles are often investigated using scanning probe microscopes which - due to their finite tip curvature - are only suited to measure roughness on a mesoscopic scale. Mesoscopic models based on an understanding of the microscopic processes [13], can bridge the gap between MD and experiment. For instance, the description of the evolution of the height profile by stochastic differential equations (SDE) [14, 15] has proved useful for the description of molecular beam epitaxy [16], sputter deposition [17] or vapour deposition [18].

For ECI-deposition, a SDE can also describe the evolution of the experimental height profile successfully as was briefly shown in [19]. The present article is intended to give a detailed derivation of this mesoscopic model. It will describe briefly the MD model for the microsopic analysis of an Energetic Cluster Impact (section 2.1). As a result, in section 2.2 two important processes will be

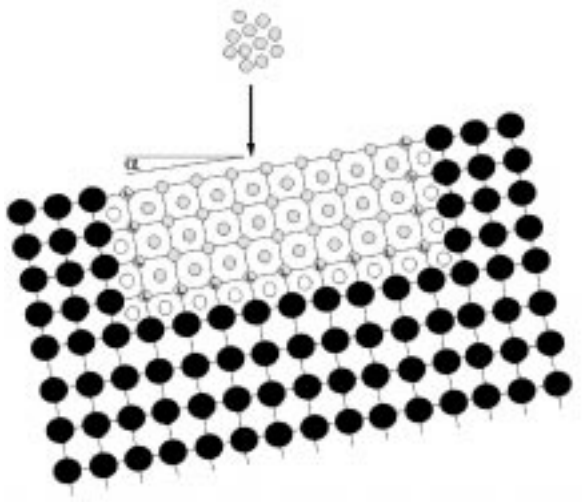

Figure 2: Schematic scetch of the MD setup. The grey atoms belong to the P zone. Their trajectories are calculated using an EAM potential. Additional Langevin-forces on the P boundary atoms (marked by an "L" in the figure) avoid the reflection of the high frequency components of the impact pressure wave and provide the thermal boundary conditions for the P zone (T=300 K). Black solid circles indicate nodes of a sc lattice in the Q zone. It serves for a discretisation of the anisotropic wave equation using finite differences. The P boundary atoms need also off-lattice information of the Q zone (white nodes), which is obtained by interpolating nearest neighbour displacements. The whole substrate is tilted by an angle α since we are interested in the impact-driven downhill particle current.

presented: a) impact-induced crater formation which influences only the nanoscale roughness and b) an additional downhill mass-transport, which is observed on sloped substrates. In section 3, the latter will form the starting point for the derivation of the SDE for the mesoscopic film profile. Finally, a comparison of this theory with available experimental data will be given.

2 Molecular Dynamics Simulations

2.1 The model

For a microscopical description of a single ECI, the trajectories $\mathbf{R}_i(t)$ of $i = 1 \dots N$ cluster and substrate atoms have to be determined. Since N is a large number ($> 10^6$ for an ECI), classical MD using an empirical interatomic potential is the only practical method for such a calculation. For metal clusters, embedded atom method (EAM) potentials [20] are usually employed to calculate the interatomic forces $\mathbf{F}_i(\mathbf{R}_1(t), \dots, \mathbf{R}_N(t))$.

The collision of an energetic cluster with a solid generates a pressure wave [8]. This wave will be reflected at the boundary of the necessarily finite simulation zone and thus artificially affects the results. Thereby, any long term prediction becomes unreliable. In a previous paper, a method was developed which allows a drastic reduction of this reflection [21]. In the following, we give a brief description of the computational scheme.

The substrate is divided into two zones (Fig. 2): the impact region or so-called primary zone (P)

contains the cluster and that part of the substrate which will be disordered by the impact. It is surrounded by a large secondary zone (Q) suffering elastic deformations only. The dynamics of the impact region is described by Newtons equation of motion

$$m\ddot{\mathbf{R}}_i(t) = \mathbf{F_i}(\mathbf{R}_1(t), \ldots, \mathbf{R}_N(t)), \quad \mathbf{R}_i(0) \; \epsilon \; \mathrm{P}. \tag{1}$$

where m is the mass of the atoms. Solving eq. (1) is the time consuming part of our computation. The motion of atoms in Q on the other hand, are calculated using

$$\mathbf{R}_i(t) = \mathbf{R}_i(0) + \mathbf{u}(\mathbf{R}_i(0), t), \quad \mathbf{R}_i(0) \; \epsilon \; \mathrm{Q}. \tag{2}$$

Here, $\mathbf{u}(\mathbf{x}, t)$ is a finite difference solution of the anisotropic wave equation

$$\rho \frac{\partial^2}{\partial t^2} u_i(\mathbf{x}, t) = C_{ikjl} \frac{\partial^2}{\partial x_k \partial x_l} u_j(\mathbf{x}, t) \tag{3}$$

where ρ is the mass density and C_{ikjl} are the elastic constants of the P system. Because of the simple structure of eq. (3), the computational costs for the Q zone are moderate and therefore it can be chosen big enough (width in the order of 100 nm) to contain the whole wave dynamics.

Boundary atoms of the P and Q zone provide boundary conditions for the Q and P zone, respectively. Since the P and Q system have the same elastic properties, no reflection of long wavelength pulses occurs at the P-Q boundary. This is not neccesarily true for high frequency waves, because the grid in the Q zone has usually a coarser spatial resolution than the atomic structure of the P-zone resulting in different short wavelength phonon dispersion relations. Reflection can be drastically reduced [21] by applying the Langevin equation

$$\begin{aligned} \frac{3}{2} m\ddot{\mathbf{R}}_i(t) &= \mathbf{F_i}(\mathbf{R}_1(t), \ldots, \mathbf{R}_N(t)) \\ &- \frac{3}{2} m\beta(\dot{\mathbf{R}}_i(t) - \dot{\mathbf{R}}_{i,\mathrm{nn}}(t)) \\ &+ \mathbf{F}_i^R(t), \quad \mathbf{R}_i(0) \; \epsilon \; \delta\mathrm{P}, \end{aligned} \tag{4}$$

to the boundary atoms of the P zone (Fig. 2). Here the damping constant is given by $\beta \approx \pi\omega_D/6$ (ω_D: Debye frequency) and $\dot{\mathbf{R}}_{i,\mathrm{nn}}$ is the average velocity of the nearest neighbours of atom i. The second term on the right hand side of eq. (4) serves as a high frequency filter since short wavelength components of the pressure wave cause motion of atoms relative to their next neighbours.

The random forces $\mathbf{F}_i^R(t)$ allow the simulation of a finite temperature substrate. The magnitude of $\mathbf{F}_i^R(t)$ is determined by the fluctuation dissipation theorem

$$< \mathbf{F}_i^R(t) \mathbf{F}_i^R(t') >= \sqrt{\frac{2\beta k_B T}{3m/2}} \delta(t - t'), \tag{5}$$

where k_B is the Boltzman constant and T the substrate temperature. In all our simulations, it has been chosen to be room temperature.

2.2 Results

The most relevant parameters for the ECI process are the size of the clusters and the impact energy. In order to determine their influence on the outcome of a single cluster impact we have performed

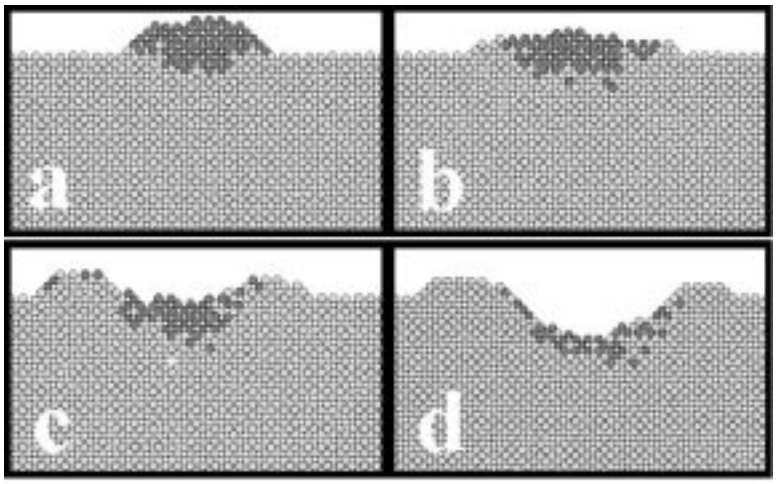

Figure 3: Final configuration after impact of a Cu_{1000} cluster onto a Cu(001) surface for different impact energies: a) 1.25 keV b) 2.5 keV c) 5 keV and d) 10 keV. A cross section in the (100) plane is displayed. The cluster atoms are represented by dark circles, the surface atoms by grey circles.

a number of simulations involving different cluster sizes (500 - 3000 atoms) and different energies (1.25 - 10 keV). For the highest energy, the P zone was a block of 42x42x21 fcc unit cells containing approximately $1.5 \cdot 10^5$ atoms. The width of the Q zone was roughly 80 nm. We recorded the atomic trajectories for up to 50 ps. This was enough time for the atoms to obtain their final positions.

As an example, fig.3 shows the final configurations for a Cu_{1000} cluster impinging with different energies onto a Cu(001)-surface. The sequence

'hill'→'plateau'→'shallow crater'→'deep crater'

occurs with increasing impact energy marking a transition from a gently sticking to a penetrating cluster. Obviously, the local roughness increases for higher energies. This seems to be in contradiction to experiment where a monotonic decrease in roughness is measured. However, the results from atomic force microscopy (fig. 1) have been obtained on mesoscopic length scales. Therefore, if one wants to explain the experimental findings one has to search for a microsopic mechanism, which, if applied repeatedly, influences the mesoscale properties of the substrate.

The single cluster experiences meso-roughness only in the occurence of a local slope of the substrate. In order to study the effect of such a slope we simulated cluster impacts onto tilted surfaces, varying the tilt angle α (fig.2) between 0° and 10°. The result for a Cu_{2000} cluster with E = 10 keV and $\alpha = 10°$ is displayed in figs. 4, 5 . It reveals the basic transport process for the mesoscopic smoothing. Immediately after the impact, an enormous pressure of 80 GPa is produced at the contact area between cluster and substrate. This pressure pulse is the driving force for crater formation and spreads out asymmetrically (fig. 5b). Since the uphill shear motion (fig. 5c) is impeded by additional surface atoms, the crater rim formation is suppressed. In the opposite direction, such an obstacle is missing allowing the rim to swash downhill (fig. 5a). It is obvious, that the impacts of many clusters will produce a downhill particle current which is an efficient means for eroding elevated features into lowerlying regions of the substrate.

Let $d_N^{(i)}$ be the displacement of atom i along the direction of the slope. A measure for the total

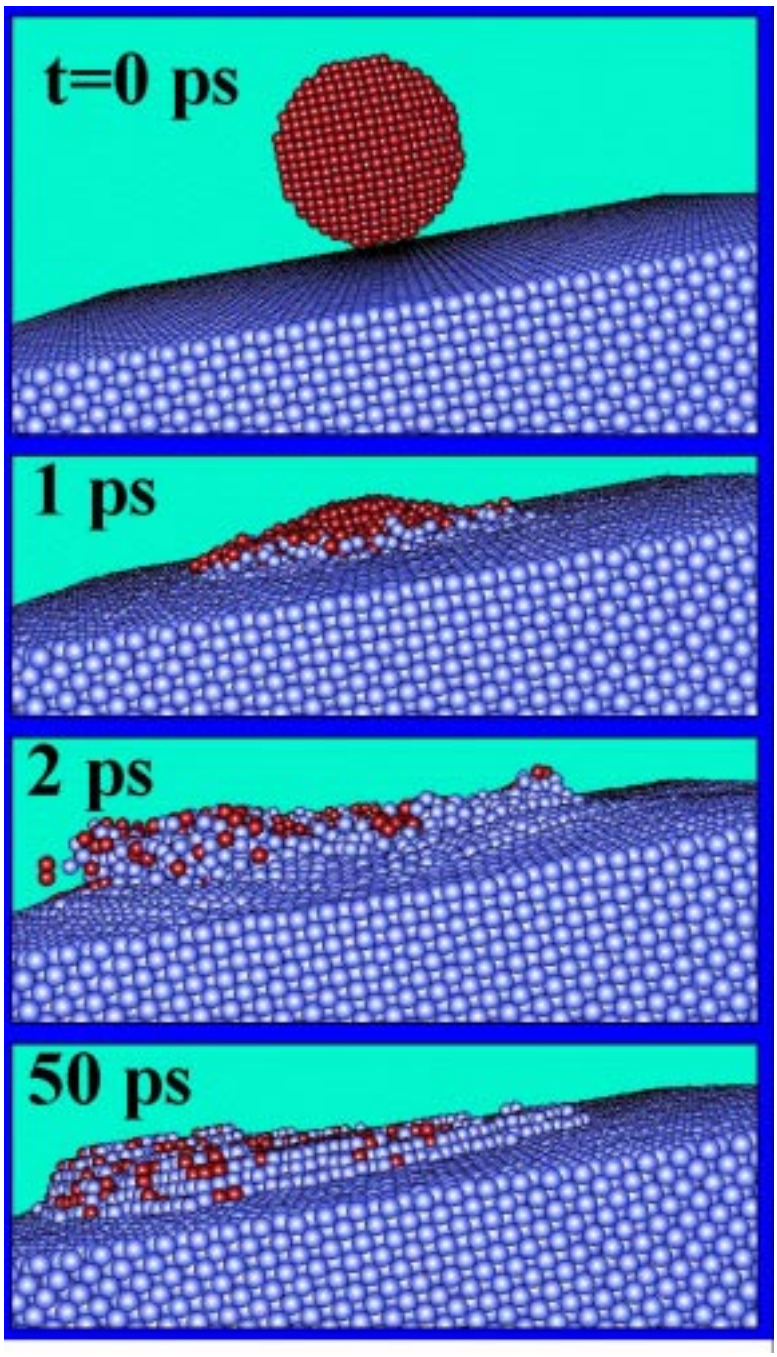

Figure 4: Snapshots of the impact of a Cu_{2000} cluster (10 keV) onto a tilted Cu(100) surface (tilt angle α=10°, cluster atoms in red and substrate atoms in blue).

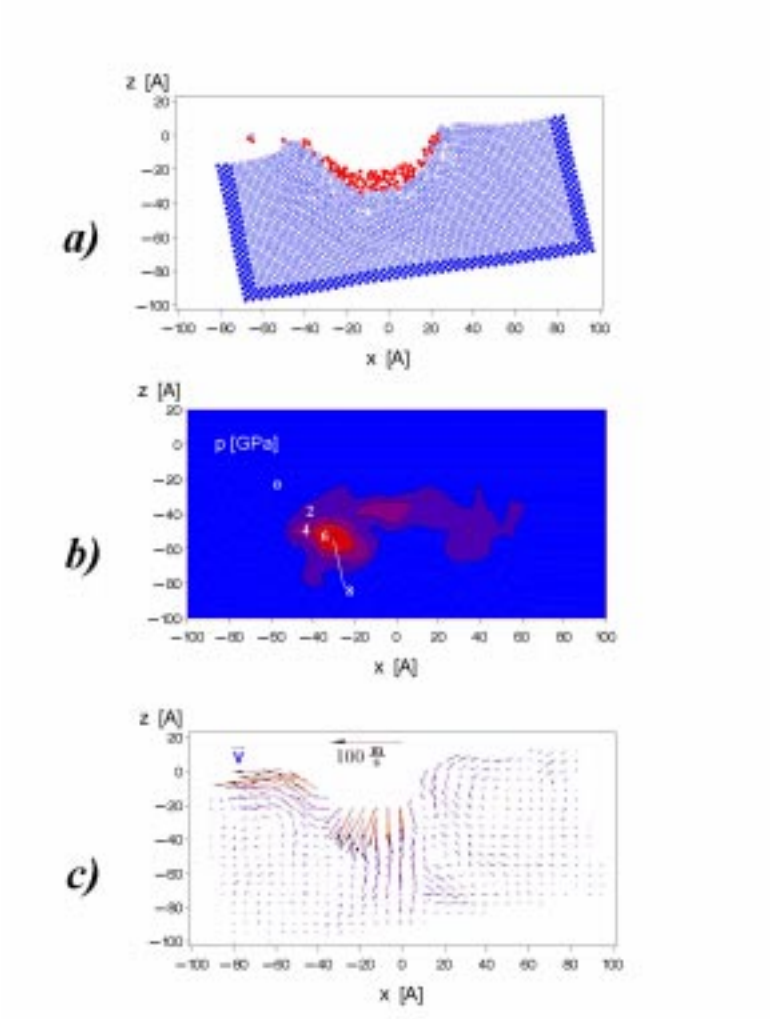

Figure 5: The impact of a Cu_{2000} cluster (10 keV) onto a tilted Cu(100) surface (same data as fig. 4). At t=3 ps an asymmetric compression can be seen a) for the atomic coordinates in a cross section through the impact center (cluster atoms in red and substrate atoms in blue) and b) in the local pressure field. The atomic velocity field in c) shows the related downhill shear motion. In order to allow a comparison, the same length scales are used in a)-c). The local fields in b) and c) were determined by distance dependent gaussian averaging of the atomic pressure and velocity components for a regular grid as described in [8, 11].

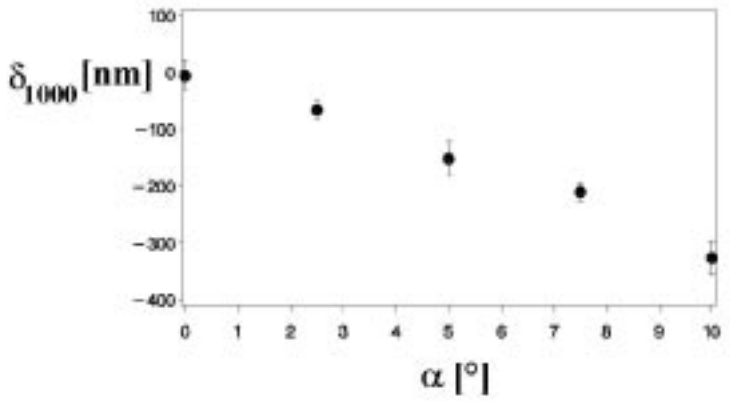

Figure 6: The dislacement sum δ_N as a function of the tilt angle α. For each α, 5 different simulations of the impact of a Cu_{1000}-cluster (1.25 keV) onto a Cu(001)-surface were performed. The crystallographic orientation of the clusters was chosen by random. The angle between the lateral component of the cluster velocity and the (100)-direction of the surface was varied between 0 and 45° in order to obtain some independence of the results from the crystal structure of the substrate [22]. The relation between δ_N and α can be considered to be linear. Because of the positive slope of the surface, atoms are moved in negative x_1 direction and therfore one has $\delta_N \leq 0$.

downhill movement of atoms is then given by the displacement sum

$$\delta_N(\alpha, E) := \sum_i d_N^{(i)}. \tag{6}$$

For a downhill movement, the displacement sum is negative. Of course, $\delta_N(\alpha, E)$ depends on the angle α of the initial slope and the impact energy E as well as the size N of the cluster. Figs. 6 and 7 show the increase of the absolute value of $\delta_N(\alpha, E)$ with increasing slope and increasing energy, respectively.

$$\delta_c \propto N\sqrt{E}. \tag{7}$$

and

$$\delta_s \propto N^{1/3}E^{4/3}. \tag{8}$$

The total displacement sum is combination of these two contributions and we end up with the formula

$$\phi_N(E) = \frac{\delta_N(\alpha, E)}{\tan\alpha} = -\left(AN\sqrt{E} + BE^{4/3}N^{1/3}\right), \tag{9}$$

with coefficients A=1.4 ± 0.1 nm/keV$^{1/2}$ and B=53 ± 2nm/keV$^{4/3}$.

Substrate atoms as well as the cluster atoms contribute to the displacement sum and in order to quantify the dependence on E and N it is useful to look at these two contributions, δ_c and δ_s, seperately. Analyzing simulations for many different sizes and energies(fig. 8), we found the empirical relations

In the following section, we show that δ is one of the main parameters for the mesoscopic description of the film growth. Thus it constitutes the link between the molcular dynamics and the mesoscopic model.

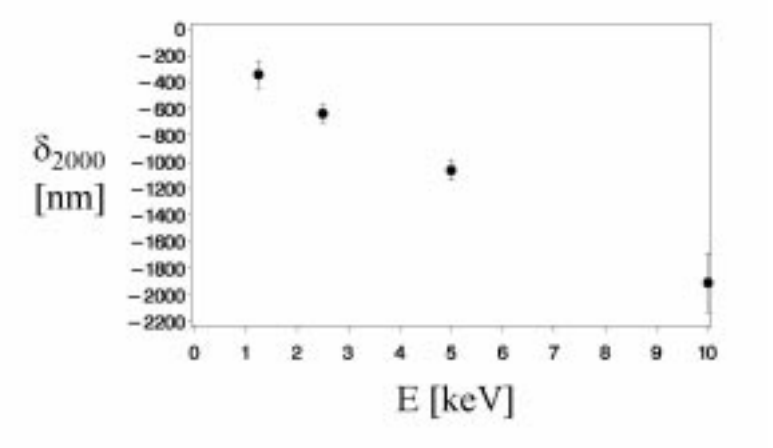

Figure 7: Displacement sum $\delta_N(\alpha{=}5°)$ for cluster size $N{=}2000$ as a function of impact energy E.

3 The Mesoscopic Model

3.1 The continuity equation

Thin films produced by ECI-deposition are dense and smooth enough to allow the neglect of cavities and overhangs. Therefore, it is possible to define the film height $h(\mathbf{x}, t)$ as a singlevalued function of the vector $\mathbf{x} = (x_1, x_2)$ in a plane parallel to the substrate (fig 9). The film material is considered to be an isotropic continuum. For constant atomic volume Ω, the number of particles in the column of volume $(\Delta x)^2 h(\mathbf{x})$ is proportional to $h(\mathbf{x})$. This particle number divided by $(\Delta x)^2$ defines a particle density ρ with respect to area by the relation

$$h(\mathbf{x}, t) = \Omega\rho(\mathbf{x}, t). \tag{10}$$

For ρ a continuity equation holds

$$\frac{\partial\rho(\mathbf{x}, t)}{\partial t} = -\nabla \cdot \mathbf{j}(\mathbf{x}, t) + \eta(\mathbf{x}, t)/\Omega, \tag{11}$$

where the particle current $\mathbf{j} = (j_1, j_2)$ describes the transition of atoms from one surface element $(\Delta x)^2$ to its neighbours. The particle source term $\eta(\mathbf{x}, t)/\Omega$ takes into account the deposition of the clusters. We insert eq. (10) into eq. (11) and obtain the equation of motion for h:

$$\frac{\partial h(\mathbf{x}, t)}{\partial t} = -\Omega\nabla \cdot \mathbf{j}(\mathbf{x}, t) + \eta(\mathbf{x}, t), \tag{12}$$

3.2 The height source

Let $n(N, \mathbf{x}, t)(\Delta x)^2 \Delta t dN$ be the number of clusters with N' atoms ($N' \epsilon [N, N{+}dN]$) falling in the time $[t, t + \Delta t]$ onto a surface element $(\Delta x)^2$ at $\mathbf{x}$. The distribution of $n(N, \mathbf{x}, t)(\Delta x)^2 \Delta t dN$ for fixed $\mathbf{x}$, t and N is binominal, since the probability for a single cluster of size N to hit the special surface element $(\Delta x)^2$ at $\mathbf{x}$ in the time intervall $[t, t + \Delta t]$ is constant. If Δx and Δt is large enough, the mean of $n(N, \mathbf{x}, t)(\Delta x)^2 \Delta t dN$ is large and therefore, the binominal is very well approximated by a gaussian

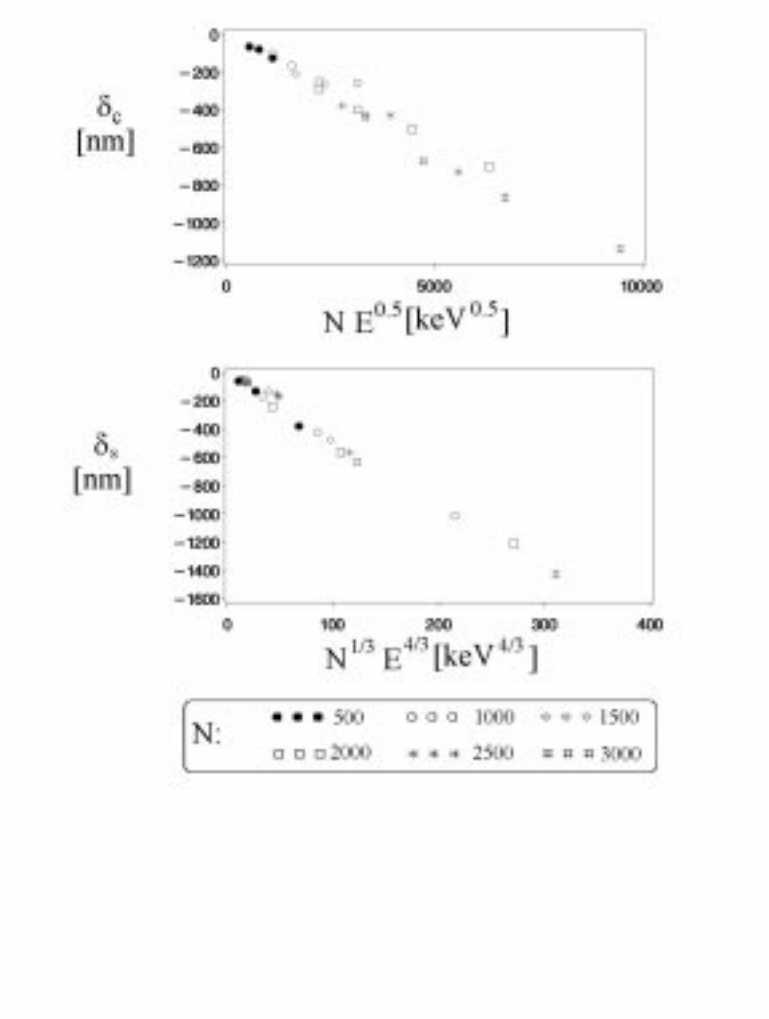

Figure 8: Cluster and substrate contribution to the displacement sum as a function of kinetic energy E and cluster size. In the simulations, the tilt angle α was 5°.

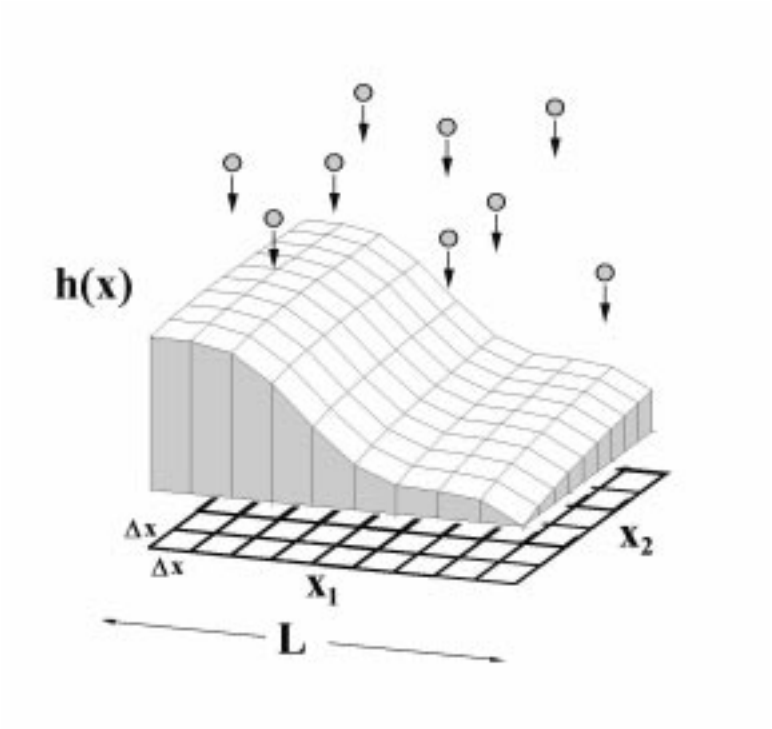

Figure 9: The surface profile is described by a single valued function **h**. The base of the substrate has an area L^2 and is devided into elements $(\Delta x)^2$ which are small compared to L^2 and large compared to the clusters' cross-sectional area.

distribution. We assume that in average r clusters arrive in unit time on a unit area and the cluster size distribution is given by the normalized probability $f(N)$. Then, the average number of clusters of size N hitting the unit surface element is given by $rf(N)dN$ and

$$\langle n(N,\mathbf{x},t)\rangle = rf(N). \tag{13}$$

Since $n(N,\mathbf{x},t)(\Delta x)^2\Delta t dN$ is a counting rate, its variance is also given by $rf(N)(\Delta x)^2\Delta t dN$. For not too small $(\Delta x)^2$, clusters falling onto element boundaries are negligible. Furthermore, the sizes and the impact points of two clusters are uncorrelated. Therefore, $n(N,\mathbf{x},t)$ and $n(N',\mathbf{x}',t')$ are uncorrelated gaussian random numbers with covariance

$$\mathrm{COV}(n(N,\mathbf{x},t),n(N',\mathbf{x}',t')) = rf(N)\delta(N-N')\delta(\mathbf{x}-\mathbf{x}')\delta(t-t'), \tag{14}$$

where the limit $\Delta t\to 0$ and $\Delta x\to 0$ has been performed. Since the height increase is given by

$$\eta(\mathbf{x},t) = \int_0^\infty dN\, N\Omega n(N,\mathbf{x},t), \tag{15}$$

we have an average height increase of

$$\langle\eta(\mathbf{x},t)\rangle = \int_0^\infty dN\, N\Omega r f(N). \tag{16}$$

and a covariance

$$\mathrm{COV}(\eta(\mathbf{x},t),\eta(\mathbf{x}',t')) = 2D\delta(\mathbf{x}-\mathbf{x}')\delta(t-t'), \tag{17}$$

with

$$D = \frac{r\Omega^2}{2}\int_0^\infty dN\, N^2 f(N). \tag{18}$$

3.3 The particle current

Consider a tilted substrate h with a tilt angle α (fig. 10):

$$h(x_1,x_2) = x_1\tan\alpha. \tag{19}$$

Assume, that a cluster with N atoms and a velocity in negative x_3 direction impinges on the origin of the substrate, and assume further, that each cluster or substrate atom j suffers a displacement from its initial location with x_1 component $x_1^{(j)}$ to its final location with x_1 component $x_1^{(j)} + d_N^{(j)}$. Caused by the downhill particle flow,

$$t_N(x_1,x_1')dx_1dx_1' = \sum_j \delta(x_1^{(j)}-x_1)\delta(x_1^{(j)}+d_N^{(j)}-x_1')dx_1dx_1' \tag{20}$$

atoms are moved from their original location in the stripe $[x_1, x_1+dx_1]$ to their final location in the stripe $[x_1', x_1'+dx_1']$. If the cluster hits instead of the origin the point (u_1,u_2), then $t_N(x_1-u_1, x_1'-u_1)dx_1dx_1'$ atoms are transported from $[x_1,x_1+dx_1]$ to $[x_1',x_1'+dx_1']$.

Now, we want to calculate the current flowing over a straight line at x_1=0 which we assume to be the boundary between a uphill and a downhill surface element. Suppose, the uphill surface element extends in the x_1 direction from 0 to $+\Delta x$ and the downhill element from $-\Delta x$ to 0, both having a width in x_2 direction of Δx.

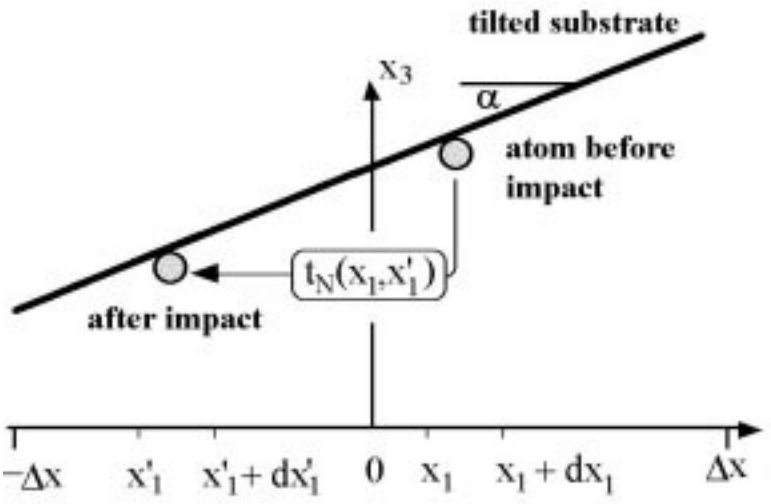

Figure 10: The impact of a N atom cluster onto a sloped substrate results in the the displacement of atoms. The number of atoms moving from $[x_1, x_1+dx_1]$ to $[x'_1, x'_1+dx'_1]$ is denoted by $t_N(x_1, x'_1)dx_1dx'_1$. The particle current passing the straight line x_1=0 is calculated using this quantity.

The clusters are falling as a homogeneous rain onto both surface elements, i.e. u_1 is a uniformly distributed random number on the intervall $[-\Delta x, \Delta x]$. For each cluster the average number of atoms passing the boundary x_1=0 is then given by

$$T_N = \int_{-\Delta x}^{\Delta x} \frac{du_1}{2\Delta x} \int_{-\infty}^{\infty} dx_1 \int_{-\infty}^{\infty} dx'_1\, t_N(x_1-u_1, x'_1-u_1)\left(\Theta(x_1)(1-\Theta(x'_1)) - (1-\Theta(x_1))\Theta(x'_1)\right), \quad (21)$$

with the heavyside funktion Θ. This can be simplified to

$$T_N = \frac{1}{2\Delta x} \int_{-\infty}^{\infty} dx_1 \int_{-\infty}^{\infty} dx'_1\, t_N(x_1, x'_1)(x'_1 - x_1). \quad (22)$$

By inserting eq. (20), the relationship between T_N and the displacement sum is found to be

$$T_N(\alpha, E) = \delta_N(\alpha, E)/(2\Delta x) \quad (23)$$

The number of clusters of size N deposited on both surface elements in unit time at the time t is $2(\Delta x)^2 n(N, \mathbf{x}=0, t)dN$ and therefore, the net number of atoms received by the downhill element is $2(\Delta x)^2 n(N, \mathbf{x}=0, t)NTdN$. A division by the length of the border line and an integration over all cluster sizes yields the particle current in the x_1 direction

$$j_1 = \int_0^{\infty} dN\, n(N, \mathbf{x}=0, t)\delta_N(\alpha, E) \quad (24)$$

One can generalize eq. (24) for a local slope in an arbitrary direction at $\mathbf{x}$. Because of symmetry, the current must be parallel to the gradient of the surface

$$\mathbf{j}(\mathbf{x}, t) = \int_0^{\infty} dN\, n(N, \mathbf{x}, t)\delta_N(|\nabla h(\mathbf{x}, t)|, E)\frac{\nabla h(\mathbf{x}, t)}{|\nabla h(\mathbf{x}, t)|}. \quad (25)$$

In MD simulations δ_N showed approximatelly a linear relationship to the tilt angle (fig. 6):

$$\delta_N(\alpha, E) = \phi_N(E)\tan(\alpha) \tag{26}$$

Therfore, the current takes the simpler form

$$\mathbf{j}(\mathbf{x}, t) = \int_0^\infty dN\, n(N, \mathbf{x}, t)\phi_N \nabla h(\mathbf{x}, t). \tag{27}$$

Using eq. (13) it can be decomposed into an average and a fluctuation contribution

$$\begin{aligned} \mathbf{j}(\mathbf{x}, t) &= \langle \mathbf{j}(\mathbf{x}, t)\rangle + \Big(\mathbf{j}(\mathbf{x}, t) - \langle \mathbf{j}(\mathbf{x}, t)\rangle\Big) \\ &= \int_0^\infty dN\, r f(N)\phi_N \nabla h(\mathbf{x}, t) + \int_0^\infty dN \Big(n(N, \mathbf{x}, t) - \langle n(N, \mathbf{x}, t)\rangle\Big)\phi_N \nabla h(\mathbf{x}, t). \end{aligned} \tag{28}$$

The related volume current is given by

$$\Omega \mathbf{j}(\mathbf{x}, t) = -\nu(1 + \zeta(\mathbf{x}, t))\nabla h(\mathbf{x}, t). \tag{29}$$

Here, the constant

$$\nu = -r\Omega \int_0^\infty dN\, f(N)\phi_N \tag{30}$$

measures the strength of the downhill transport and the random numbers

$$\zeta(\mathbf{x}, t) = \frac{\int_0^\infty dN \Big(n(N, \mathbf{x}, t) - \langle n(N, \mathbf{x}, t)\rangle\Big)\phi_N}{r\int_0^\infty dN\, f(N)\phi_N} \tag{31}$$

take into account the current fluctuations due to the randomly deposited clusters.

3.4 The comoving frame

The velocity v_s of the mean film height

$$s(t) = \frac{1}{L^2}\int d^2x h(\mathbf{x}, t) \tag{32}$$

is given by eq. (16). We introduce a new frame comoving with the growing film i.e.with a velocity v_s in the x_3 direction. In this new reference frame no height sources are present

$$\langle n(N, \mathbf{x}, t)\rangle = 0, \tag{33}$$

which implies

$$\langle \eta(\mathbf{x}, t)\rangle = 0, \tag{34}$$

$$\langle \eta(\mathbf{x}, t)\eta(\mathbf{x}', t')\rangle = 2D\delta(\mathbf{x} - \mathbf{x}')\delta(t - t'), \tag{35}$$

and

$$\zeta(\mathbf{x}, t) = \frac{\int_0^\infty dN\, n(N, \mathbf{x}, t)\phi_N}{r\int_0^\infty dN\, f(N)\phi_N}. \tag{36}$$

Now, the covariance of η and ζ is given by

$$\langle \eta(\mathbf{x},t)\zeta(\mathbf{x}',t')\rangle = 2D_{\eta\zeta}\delta(\mathbf{x}-\mathbf{x}')\delta(t-t') \quad (37)$$

$$\langle \zeta(\mathbf{x},t)\zeta(\mathbf{x}',t')\rangle = 2D_{\zeta\zeta}\delta(\mathbf{x}-\mathbf{x}')\delta(t-t'). \quad (38)$$

Here, the eqns. (14), (15) and (36) were used and

$$D_{\eta\zeta} = \frac{\Omega \int_0^\infty dN\, f(N)\phi_N N}{2\int_0^\infty dN\, f(N)\phi_N} \quad (39)$$

$$D_{\zeta\zeta} = \frac{\int_0^\infty dN\, f(N)\phi_N^2}{2r(\int_0^\infty dN\, f(N)\phi_N)^2}. \quad (40)$$

3.5 The Edwards-Wilkinson equation

By introducing eq. (29) into eq. (12) one obtains a closed equation of motion for h

$$\frac{\partial h(\mathbf{x},t)}{\partial t} = \nu\nabla(1+\zeta(\mathbf{x},t))\nabla h(\mathbf{x},t) + \eta(\mathbf{x},t). \quad (41)$$

The multiplicative noise $\nabla(\zeta\nabla h)$ takes into account the dependence of the lateral current on fluctuations of the local deposition rate.

Irrespective of the cluster-induce downhill current, other types of lateral mass transport are possible on a rough surface [23]: viscous flow, desorption, volume diffusion and surface diffusion. All these processes are also active if atoms instead of clusters are added to the surface, but none of them depends on the deposition rate. The strength of these processes can be calculated from known material constants [23]. For copper at room temperature the influence of viscous flow, desorption and volume diffusion can be ruled out immediately because of a tremendous viscosity, a very low vapour pressure and a very small volume difussion coefficient. Only surface diffusion may influence the small wavelength modes of h. Following [23], we extend eq.(41) to

$$\frac{\partial h(\mathbf{x},t)}{\partial t} = \nu\nabla^2 h(\mathbf{x},t)) + \nu\nabla(\zeta(\mathbf{x},t)\nabla h(\mathbf{x},t)) - K\nabla^4 h(\mathbf{x},t) + \eta(\mathbf{x},t), \quad (42)$$

with a coefficient K measuring the strength of surface diffusion. This rather complicated equation simplifies drastically in the hydrodynamic limit [13], i.e. for large length and time scales. If one performs the following scale transformation for $b>0$

$$\tilde{h}(\mathbf{x},t) = b^{-\alpha}h(b\mathbf{x}, b^z t), \quad (43)$$

powercounting, i.e. the comparison of the various b-exponents occuring in the scaled SDE, shows that the second and third term on the right hand side of eq. (42) vanish in the limit $b\to\infty$. What remains is the so-called Edwards-Wilkinson (EW) equation

$$\frac{\partial h(\mathbf{x},t)}{\partial t} = \nu\nabla^2 h(\mathbf{x},t) + \eta(\mathbf{x},t) \quad (44)$$

which was originally discovered in the context of sedimentation [24].

Often, SDEs also include additional nonlinear terms [13]. However, all conceivable nonlinearities which are consistent with the conserved nature of the dynamics can be shown to be irrelevant (compared to $\nabla^2 h$) in the hydrodynamic limit [15]. Thus, our linear theory provides the exact description of the large scale properties.

Many experiments record the average film height $s{=}v_s t$ instead of the deposition time. This variable transformation does not alter the structure of eq. (44) :

$$\frac{\partial h(\mathbf{x},s)}{\partial s} = \nu \nabla^2 h(\mathbf{x},s) + \eta(\mathbf{x},s). \tag{45}$$

However, the parameter

$$\nu = -\frac{\int_0^\infty dN\, f(N)\phi_N}{\int_0^\infty dN\, f(N)N}. \tag{46}$$

changes. Furthermore, for the new source term $\eta(\mathbf{x},s)$

$$< \eta(\mathbf{x},s)\eta(\mathbf{x}',s') >= 2D\delta(\mathbf{x}-\mathbf{x}')\delta(s-s') \tag{47}$$

with

$$D = \frac{\Omega \int_0^\infty dN\, N^2 f(N)}{2\int_0^\infty dN\, N f(N)}. \tag{48}$$

holds.

According to the Edwards-Wilkinson quation, the film growth is determined solely by D und ν which in turn depend only on the cluster size distribution $f(N)$ (known from time-of-flight experiments) and the displacement sum δ_N.

3.6 Solution of the Edwards-Wilkinson Equation

In fourier space, eq. (45) takes the form

$$\frac{dh_{\mathbf{k}}(s)}{ds} = -\nu k^2 h_{\mathbf{k}}(s) + \eta_{\mathbf{k}}(s) \tag{49}$$

with

$$\left\langle \eta_{\mathbf{k}}(s)\eta_{\mathbf{k}'}(s') \right\rangle = \delta(s-s')\delta_{\mathbf{k},-\mathbf{k}'}\frac{2D}{L^2}. \tag{50}$$

From the formal solution

$$h_{\mathbf{k}}(s) = e^{-\nu k^2 s} h_{\mathbf{k}}(0) + \int_0^s ds'\, \eta_{\mathbf{k}}(s') e^{-\nu k^2 (s-s')} \tag{51}$$

one can calculate the power spectrum

$$\tilde{C}(k,s) = \left\langle h_{\mathbf{k}}(s) h^*_{\mathbf{k}}(s) \right\rangle = e^{-2\nu k^2 s}\tilde{C}(k,0) + \frac{D}{\nu L^2 k^2}\left(1 - e^{-2\nu k^2 s}\right). \tag{52}$$

Note, that for initially rough surfaces the first term in eq. (52) vanishes exponentially, which indicates the possibility to smooth a rough surface by ECI coating.

3.7 Comparison with experiments

Assuming initially flat substrates, i.e. $\tilde{C}(k,0) = 0$, we have fitted eq. (52) to experimental power spectra of films produced by depositing negative Cu cluster ions having a mean size of 2000 atoms/cluster with 10 keV onto a Si(001) substrate (fig.11). Details of our experimental setup for Energetic Cluster Impact (ECI) deposition are published elsewhere [3]. The cluster size distribution was measured with

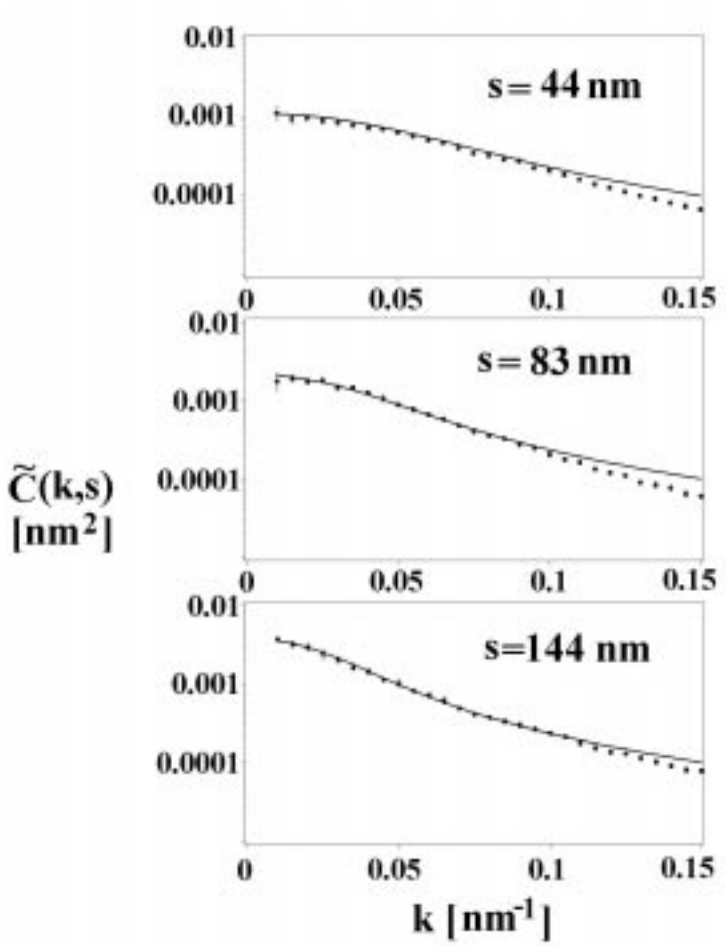

Figure 11: Comparison of experimental power spectra (dots) with the Edwards-Wilkinson power sprectrum (lines). The good agreement between experiment and theory for different film thicknesses indicates that the dynamics of long wavelength modes is governed by the Edwards-Wilkinson equation.

a time-of-flight mass spectrometer which allows to calculate an experimental value for D according to eq. (48) . Power spectra of the Cu films have been calculated from Atomic Force Microscopy (AFM) images using a Nanoscope III in the tapping mode. Besides from leveling the three-dimensional AFM data in order to compensate for subtrate tilt no other filtering was applied.

The fit to the experimental power spectra revealed D=13 $\pm$ 0.5 nm^3 and ν=7 $\pm$ 1 nm. The source strength D is in good agreement with the experimental value D=15 $\pm$ 1 nm^3. In order to check the exponent of k an additional parameter ϵ was introduced changing k^2 to $k^{2+\epsilon}$. The result ϵ=0.1 $\pm$ 0.1 confirmed the ∇^2 term in the growth equation. For k>0.1 nm^{-1}= k_0 the experimental mode strength is smaller than the theoretical one. This can be explained by a deviation from the hydrodynamic limit i.e. for higher k surface diffusion and the fluctuations of the local deposition rate become more and more important. The downhill strength obtained from the MD-simulations for Cu_{2000} clusters is given by

$$\nu = -\frac{\delta_{2000}(\alpha, 10 \text{ keV})}{2000 \tan \alpha} = 10.9 \pm 1.3nm \tag{53}$$

which is in good agreement with the experimental value of ν=7$\pm$1 nm. Using eqs. (9) and (46), ν can be completely expressed in terms of the fundamental ECI-parameters:

$$\nu = A\sqrt{E} + BE^{4/3}\frac{\langle N^{1/3}\rangle}{\langle N\rangle}. \tag{54}$$

Thus, the influence of the cluster size distribution and the impact energy on the film roughness can be predicted.

3.8 Evolution of surface roughness

The root mean square (RMS) roughness R of the film is given by

$$R(s)^2 = \left\langle \frac{1}{L^2}\int dx^2 \left(h(\mathbf{x}, s) - s\right)^2 \right\rangle = \sum_{\mathbf{k}\neq 0} \tilde{C}(\mathbf{k}, s). \tag{55}$$

The second equality follows from $R(s)^2$=$C(\mathbf{x}$=$0, s)$, where C is the fourier transform of $\tilde{C}$. In the co-moving frame $\eta_{\mathbf{k}=0}$ and consequently $C(\mathbf{k}$=$0, s)$ vanishes. Since the validity of the EW powerspectrum is limited to k<k_0 the RMS roughness should be decomposed into two parts

$$R^2 = R_<^2 + R_>^2 = \sum_{\mathbf{k},|\mathbf{k}|\leq k_0} \tilde{C}(k_1, k_2) + \sum_{\mathbf{k},|\mathbf{k}|>k_0} \tilde{C}(k_1, k_2), \tag{56}$$

where the component $R_<$ takes into account the roughness of the hydrodynamic modes. For all three films in fig. 11, $R_<$ was roughly 85% of the total R. Therefore, it is sufficient to study the hydrodynamic roughness $R_<$ in order to explain experimental trends.

For an initially flat height profile

$$R_<^2 = \int_{\pi/L}^{k_0} dk\, \frac{D}{2\pi\nu k}\Big(1 - e^{-2\nu k^2 s}\Big), \tag{57}$$

can be solved analytically

$$R_<^2 = \frac{1}{2}\frac{D}{2\pi\nu}\left[2\ln\left(\frac{Lk_0}{\pi}\right) + \text{Ei}(-2\nu s\pi^2/L^2) - \text{Ei}(-2\nu s k_0^2)\right] \tag{58}$$

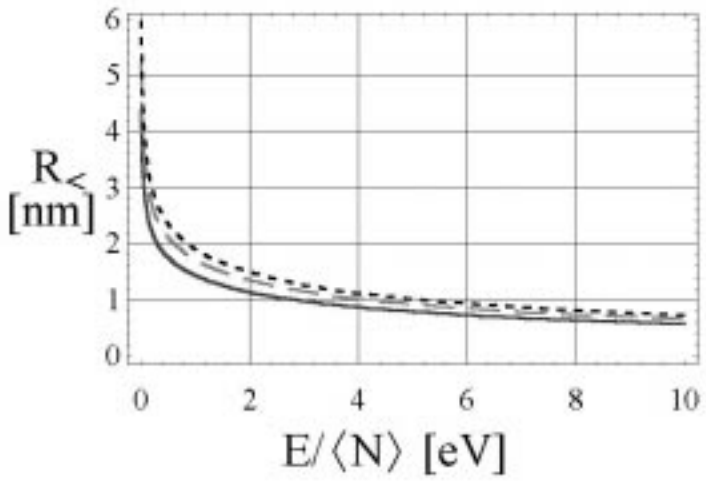

Figure 12: Theoretical hydrodynamic roughness $R_<$ as a function of the impact energy per atom for three cluster sizes: 1000 atoms (solid line), 2000 atoms (long dashes) and 3000 atoms (short dashes). For constant E/N the roughness is nearly independent of cluster size.

By inserting eq. (54) and (18) into eq. (58) and assuming a peaked cluster size distribution, one can calculate the dependence of the RMS roughness on the kinetic energy and the cluster size. In fig 12, $R_<$ is plotted as a function of impact energy per cluster atom for different cluster sizes. The hydrodynamic roughness $R_<$ is dominated by E/N and at constant E/N depends only weakly on N. For $E/N<1$ eV a large roughness is predicted. It decreases drastically for $E/N\leq 2$ eV. A further increase of E/N results in a slight reduction of $R_<$. These theoretical findings are in a good qualitative agreement with the overall experimental trend (fig. 1).

For an initially rough substrate, a term

$$\int_{\pi/L}^{k_0} dk\, \frac{L^2}{2\pi} k e^{-2\nu k^2 s} \tilde{C}(k,0) \tag{60}$$

has to be added to eq. (58), which describes the exponential decay of the initial power spectrum. Thus, the initial hydrodynamic roughness also decays exponentially with the thickness of the deposited film (fig. 13). For large thicknesses, it converges to the roughness of a corresponding film with zero initial roughness.

with the integral exponential function Ei. For not too large s, $R_<$ can be approximated by

$$R_<^2 = \frac{1}{2}\frac{D}{2\pi\nu}\Big[\ln\left(2\nu k_0^2 s\right) + C\Big] \tag{59}$$

with the Euler-Mascheroni constant C. This logarithmic relationship explains the smoothness of the ECI-films. It is a unique feature of the EW equation [13, 15] since other growth equations show an algebraic increase of roughness with growing film heigth.

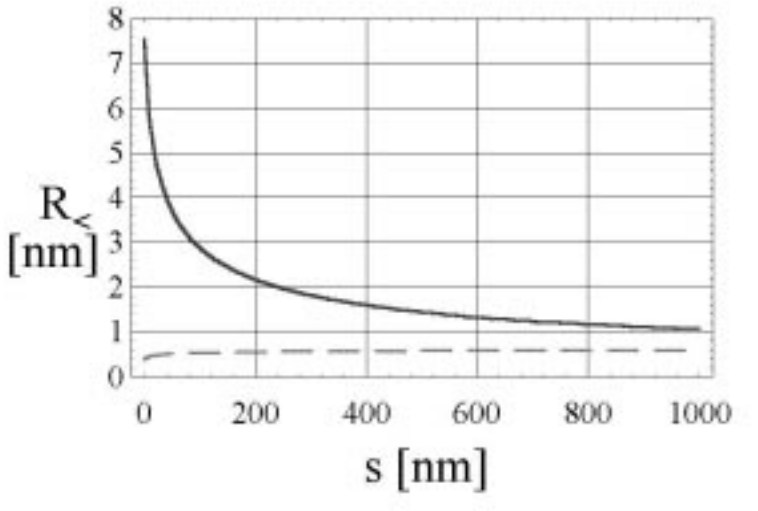

Figure 13: Theoretical hydrodynamic roughness $R_<$ as a function of the film thickness s for an initialy rough (solid line) and a flat (dashes) substrate. The rough substrate is thought to be produced by low energy deposition of very large clusters i.e. the power spectrum $C(k,0)$ of this initial 1000 nm thick film is assumed to be of the EW type with the very unfavourable parameter choice D_0=100 nm^3 and ν_0=1 nm. After that a film of Cu_{1000} with 10 keV was deposited. The rapid decrease of the roughness indicates the smoothing capability of the ECI process.

4 Conclusions

The smoothness of thin films produced by ECI-deposition can be explained by a downhill mechanism occuring on a sloped part of the substrate. In MD simulations, the related particle current increases considerably with increasing impact energy, a trend which is also observed in experiment. The RMS roughness decreases with increasing kinetic energy per cluster atom. This indicates two possiblities to prepare smoother thin films: to use a) higher impact energies or b) smaller cluster sizes.

However, for too high impact energies the crater width may become comparable to the long wavelength modes of the surface increasing the mesoscopic roughness. On the other hand, too small clusters may penetrate deeply into the solid causing radiation damage. This should be taken into accont in the search for an optimum setup of ECI experiments. The width of the cluster size distribution should be as small as possible, since roughness is linearly related to the variance D of the deposition noise and consequently to the cluster size range.

For ECI-deposition on rough substrates an exponential decay of the initial roughness is predicted. Therefore, energetic cluster impacts may also be used for surface smoothing. Experiments are on the way to confirm this prediction.

References

[1] Ion Beam Assisted Film Growth, ed. by T.Itoh, (Elsevier, Amsterdam, 1989)

[2] W.Brown, M.Sosnowski, Nucl. Instrum. and Methods B **102**, 305 (1995)

[3] H.Haberland, M.Karrais, M.Mall, and Y.Thurner, J. Vac. Sci. Technol. A 10, 3266 (1992);
H.Haberland, M.Moseler, Y.Qiang, O.Rattunde, T.Reiners, and Y.Thurner, Surf. Rev. & Let. **3**, 887 (1996);
Y.Qiang, Y.Thurner, T.Reiners, O.Rattunde, and H.Haberland, Surf. Coat. Technol. 100-101, 27 (1998))

[4] K.Müller, J. Appl. Phys. **61**, 2516 (1987)

[5] I.Kwon, R.Biswas, G.S.Grest and C.M.Soukoulis, Phys. Rev. B **41**, 3678 (1990)

[6] H.Hsieh, R.S.Averback, H.Sellers, and C.P.Flynn, Phys. Rev. B **45**, 4417 (1992)

[7] J.D.Pelletier, M.H.Shapiro, and T.A.Tombrello, Nucl. Instrum. and Methods B **67**, 256 (1992)

[8] C.L.Cleveland and U.Landmann, Science **257**, 355 (1992)

[9] D.Fenyo, B.U.R.Sundqvist, B.R.H.Karlsson, Phys.Rev. B, **42**, 1895 (1990);
K.Barghorn, E.R.Hilf, Nucl. Instrum. and Methods B **88**, 196 (1994);
H.P.Cheng and U.Landman, J. Chem. Phys. **98**, 3527 (1994);
G.Vandoni, C.Felix,and C.Masobrio, Phys.Rev. B **54**, 1553 (1996);
I.Schek and J.Jortner, Chem. Phys. Lett. **257**, 273 (1996);
Z.Insepov, I. Yamada, Nucl. Instrum. and Methods B **121**, 44 (1997);
G.Betz and W.Husinsky, Nucl. Instrum. and Methods B **122**,311 (1997);
R.P.Webb, M.Kerford, M.Kappes, and G.Brauchle, Nucl. Instrum. and Methods B **122**,318 (1997);
G.Gilmer, C.Roland, D.Stock, M.Jaraiz, T. Diaz de la Rubia, Materials Science & Engineering B **37**, 1 (1996)

[10] H.Haberland, Z.Insepov, and M.Moseler, Z.Phys. D **26**, 229 (1993)

[11] H.Haberland, Z.Insepov, and M.Moseler, Phys. Rev. B **51**, 11061 (1995)

[12] M.Moseler, J.Nordiek, O.Rattunde and H.Haberland, Radiation Effects **142**, 38 (1997)

[13] A.L.Barabasi, and H.E.Stanley, Fractal Concepts in Surface Growth (Cambridge University Press, Cambridge 1995)

[14] J.Villain, J. Phys. I **1**,19 (1991)

[15] J.Krug, Advances in Physics **46**, 139 (1996)

[16] D.E.Wolf and J.Villain, Europhys. Lett., **13**, 389 (1990);
S.DasSarma and P.Tamborea, Phys. Rev. Lett. **66**, 325 (1991);
Z.W.Lai and S.DasSarma, Phys. Rev. Lett. **66**, 2348 (1991)

[17] R.P.U.Karunasiri, R,Bruinsma, K.Rudnick, Phys. Rev. Lett. **62**, 788 (1989)

[18] M.Kardar, G.Parisi, and Y.Zhang, Phys. Rev. Lett., **56**, 889 (1986)

[19] M.Moseler, O.Rattunde , J.Nordiek, and H.Haberland, Comp. Mat. Science **10**, 452 (1998)

[20] We used: D.J.Oh and R.A.Johnson, J. Mater. Res. **3**, 471 (1988)

[21] M.Moseler, J.Nordiek, and H.Haberland, Phys. Rev. B **56**, 15439 (1997)

[22] That the cristallographic orientation of the substrate has some influence on the crater shape was shown by J.Nordiek, M.Moseler, and H.Haberland, Radiation Effects **142**, 27 (1997)

[23] W.W. Mullins, J. Appl. Phys. **30**, 77 (1959), W.W. Mullins, J. Appl. Phys. **28**, 333 (1957)

[24] S.F.Edwards and D.R.Wilkinson,Proc. R. Soc. Lond. A **381**, 17 (1982)